Algorithm for Inferring Wind Stress from SeaSat-A

W. Linwood Jones*
NASA Langley Research Center, Hampton, Va.
Frank J. Wentz†
Frank J. Wentz and Associates, San Francisco, Calif.
and
Lyle C. Schroeder‡
NASA Langley Research Center, Hampton, Va.

On the SeaSat-A satellite, a microwave scatterometer will be used to infer the wind vector over the world's oceans. This paper describes an algorithm to convert the scatterometer's normalized radar cross-section measurements to sea-surface wind stress and neutral stability wind vector. The algorithm is based on experimental NRCS data from aircraft measurements and a two-scale radar-scattering model. The technique uses Bayes' probabilistic equation to infer the friction velocity vector, from which the wind stress and neutral stability wind vectors are determined. Two examples of inverted radar data are presented: 1) a comparison of aircraft-radar-inferred friction velocity vector to that derived from surface wind measurements in the New York Bight and 2) a simulated SeaSat-A measurement inversion in which comparisons are made of the recovered and sample wind fields.

Introduction

IN June 1978, an experimental oceanographic satellite known as SeaSat-A was launched. The objectives of this satellite program have been established through strong oceanographic and meteorological user participation[1,2] and include the ocean global measurement of the marine geoid, surface wind vectors, surface temperature, wave heights, and spectra. The SeaSat-A global and synoptic view of these and other biological and physical ocean characteristics should be of much value to the scientific community.[3] SeaSat-A is unique in that it carries a complement of active and passive microwave remote sensors as well as a visible/infrared radiometer. One active microwave sensor, the SeaSat-A satellite scatterometer (SASS), will be used to infer the wind stress and the neutral stability wind vector over the world's oceans.[4] (Neutral stability wind speed is defined as the wind speed that would result from a given friction velocity if the atmosphere were neutrally stratified. Hence the neutral stability wind speed and the friction velocity are uniquely related.)

Microwave scatterometers have been shown to be sensitive to surface winds in previous aircraft programs[5-7] and the Skylab S-193 experiment.[8] This results from the Bragg scattering of microwaves from capillary ocean waves, the amplitudes of which are in turn a function of the friction velocity, U_*. Friction velocity is a vector parallel to the sea surface in the downwind direction with magnitude $U_* = \sqrt{\tau/\rho}$, where τ is the surface wind stress and ρ is the density of the air. A recent study[9] demonstrated that the ocean's normalized radar cross section (NRCS) increases with U_* for radar incidence angles greater than about 20 deg. Furthermore, the NRCS is anisotropic and information on the wind direction can be obtained from scatterometer measurements having orthogonal azimuth angles. For SeaSat-A, specifications for the scatterometer have developed from requirements of the SeaSat User Working Group: viz., wind-speed-measurement range of 4 to >24 m/s with an accuracy of ±2 m/s or ±10% whichever is greater; wind direction 0-360 deg ±20 deg; 1000-km swath; 50-km resolution cell; cross-track and along-track spacing between resolution cells of 100 km.

From a number of scatterometer design options ranging from pencil-beam to fan-beam, the fan-beam approach was chosen.[4] The SASS incorporates four dual-polarized antennas which produce an x-shaped illumination pattern on the surface (Fig. 1). The peak of each antenna beam is centered at a 47-deg incidence angle. This beam location favors the outer swath section, where the received signals are weaker because of an increased range and a lower sea NRCS. Fifteen Doppler filters and range gates are used to electronically subdivide the antenna fan-beam into separate resolution cells. Three Doppler cells provide measurements at Earth incidence angles of 0, 4, and 8 deg to form the 140-km measurement swath centered about the satellite subtrack. Twelve additional Doppler cells provide NRCS measurements at Earth incidence angles from about 25-65 deg on each side of the subtrack. The region labeled "high winds only" (Fig. 1) is for incidence angles between 55-65 deg. Here the return signals should be large enough to detect only if the winds exceed 10 m/s. This paper describes the development of an algorithm to infer the friction-velocity vector U_* from these two radar measurements.

Algorithm Experimental Data Base

The SASS geophysical algorithm which converts NRCS measurements to the friction velocity vector U_* requires a comprehensive set of radar/anemometer data. These data were obtained during aircraft experiments in which the aircraft flew an assortment of straight lines and circles. A data base of the NRCS was collected for a variety of incidence angles and azimuth angles relative to the wind direction. Sea-surface anemometer measurements were made simultaneously with the NRCS measurements, thereby allowing for correlations to be established between the NRCS measurements and U_*. The measurements were obtained under a variety of conditions ranging from light winds and calm seas to gale conditions. For each flight, the local wind

Received Nov. 14, 1977; presented as Paper 77-1614 at the AIAA/AGU/AMS/IEEE/MTS/SEG Conference on Satellite Applications to Marine Operations, New Orleans, La., Nov. 15-17, 1977; revision received May 5, 1978.

Index categories: Oceanography, Physical and Biological; Data Sensing, Presentation, and Transmission.

*SASS Experiment Scientist.

†President.

‡Aerospace Technologist.

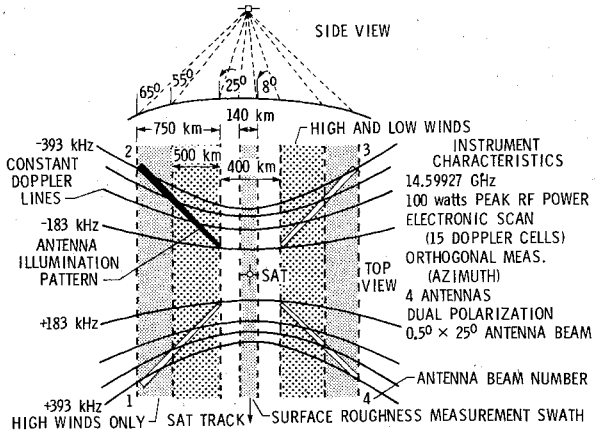

Fig. 1 SASS illumination pattern.

vector and the atmospheric stability (air/sea temperature difference) were measured by either in situ or airborne sensors. The measured wind speed was extrapolated to the surface using a boundary-layer wind model[10] and the friction velocity U_* was computed.

The data were obtained in the Gulf of Mexico and the North Atlantic during 1973-1974[5] and the North Sea (JONSWAP§) during 1975. To obtain information on the anisotropic scattering characteristics of the NRCS the aircraft was flown in a series of high-banked 360-deg turns. This caused the antenna to be conically scanned over the ocean surface. This procedure resulted in measurements being obtained over an incidence angle range of 20 to 65 deg for both vertical and horizontal polarization. The measurements were averaged in azimuth over 10-deg sectors, and typically five or more circles were flown to obtain a statistically representative sample. The anisotropic scattering characteristics for three flights are shown in Fig. 2 in which σ^0 denotes the NRCS measurements. The abscissa is the radar azimuth relative to the crosswind direction. This figure demonstrates that σ^0 increases with high wind speeds. The anisotropic characteristic is a quasi-sine of twice the azimuth angle curve with peaks at the upwind and downwind directions and with the minima at the crosswind direction. These data also show an upwind/downwind asymmetry where the upwind peak is slightly greater than the downwind peak.

Additional radar scatterometer data were obtained in straight-and-level flight lines flown in a constant direction relative to the surface winds. Typical flight lines were of 50-km length and 8-min duration. During these lines, the scatterometer polarization alternated between vertical and horizontal, and the antenna elevation angle was stepped six positions between nadir and approximately 52 deg. A typical example of the data is shown in Fig. 3 where the mean value of σ^0 for constant incidence angles are plotted versus the neutral stability 19.5-m wind speed. Here the neutral stability wind speed is used rather than the friction velocity to be consistent with previous investigations. The typical sensitivity of σ^0 to incidence angle and wind speed is demonstrated in Fig. 3.

The NRCS Model

The NRCS model is based on the two-scale scattering theory. In particular, the scatterometer footprint is segmented into regions having dimensions large compared to the radiation wavelength. These regions will, in general, be tilted with respect to the mean surface across the footprint. A tilt probability is assigned, and the overall NRCS is found by integrating over the regional NRCS weighted by the tilt probability and a geometric factor necessary to ensure energy conservation. Furthermore, the NRCS for a particular region depends upon the wavenumber spectrum of the sea-surface

§Joint North Sea Wave Project.

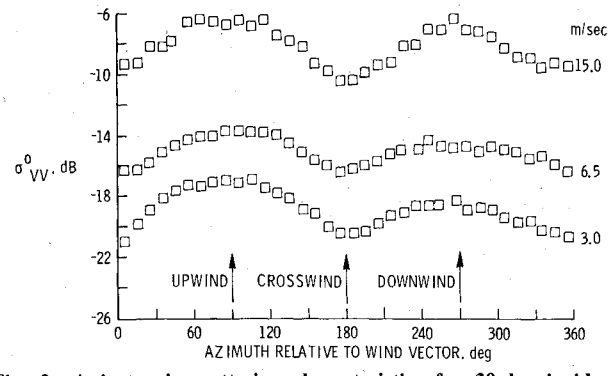

Fig. 2 Anisotropic scattering characteristics for 30-deg incidence angle measurements during flights at three different wind speeds.

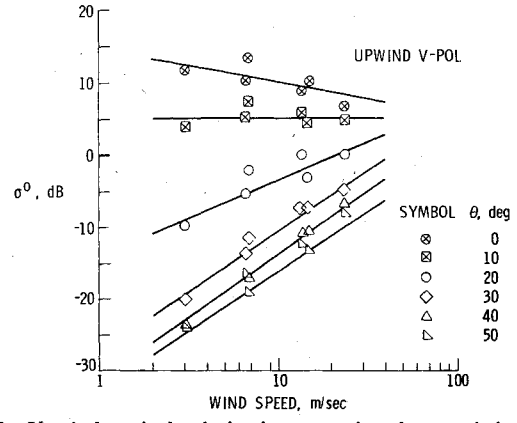

Fig. 3 Upwind vertical polarization scattering characteristics vs wind speed as a function of incidence angle.

roughness within the region. This dependence is due to Bragg scattering by sea waves having wavenumbers similar to the radiation wavenumbers.

The formulation for the model is given by Wentz[11] and results in the NRCS being a function of the following inputs: 1) the radiation wavenumber k; 2) the permittivity ϵ of sea water; 3) the unit vector $\boldsymbol{k}_i$ pointing from the scatterometer to the footprint; 4) the unit polarization vector $\boldsymbol{E}_i$; 5) the unit normal $\boldsymbol{N}$ of the mean surface across the footprint; 6) the probability density function (pdf) $P_n(\boldsymbol{n})$ of the regional normal unit vector $\boldsymbol{n}$; 7) the wavenumber spectrum $F(\boldsymbol{K},\boldsymbol{n})$ of the sea-surface roughness within a region having a normal $\boldsymbol{n}$ ($\boldsymbol{K}$ = vector wavenumber); and 8) the power reflection coefficient R for normal incidence.

The first five inputs are known quantities. The two distributions, $P_n(\boldsymbol{n})$ and $F(\boldsymbol{K},\boldsymbol{n})$ are functions of the following implicit arguments: the mean normal $\boldsymbol{N}$, the sea-surface friction velocity vector $\boldsymbol{U}_*$, and a number of model parameters that are described below. The spectrum $F(\boldsymbol{K},\boldsymbol{n})$ is normalized such that its integral over all $\boldsymbol{K}$ equals the mean-squared height variation. The power reflection coefficient R is a modification of the Fresnel power reflection coefficient for normal incidence and accounts for the reduction in reflected power due to Bragg scattering.

The pdf for the regional normals is given by

$$P_n(\boldsymbol{n}) = (\boldsymbol{n}\cdot\boldsymbol{N})^{-3} P_s(S_u, S_c) \tag{1}$$

$$S_u = \boldsymbol{n}\cdot\boldsymbol{U}_* / [U_*(\boldsymbol{n}\cdot\boldsymbol{N})] \tag{2}$$

$$S_c = \boldsymbol{n}\cdot\boldsymbol{N}\times\boldsymbol{U}_* / [U_*(\boldsymbol{n}\cdot\boldsymbol{N})] \tag{3}$$

where $U_* = |\boldsymbol{U}_*|$ and $P_s(S_u, S_c)$ is the pdf for the upwind and crosswind regional slopes, S_u and S_c. The factor $(\boldsymbol{n}\cdot\boldsymbol{N})^{-3}$ is the Jacobian relating the differential area $dS_u\, dS_c$ to the differential solid angle $d\boldsymbol{n}$. The slope pdf is assumed to be a

Gaussian,[12] having zero mean and standard deviations $\bar{S}_u$ and $\bar{S}_c$ for the upwind and crosswind slopes. Some error in the model's anisotropy may be introduced if the slope pdf is significantly skewed. However, the peakedness and higher order moments can probably be safely neglected.[13]

The region $k/2<K<2k$ $(K=|\boldsymbol{K}|)$ of the wavenumber spectrum $F(\boldsymbol{K},n)$ is responsible for Bragg backscattering. For the SASS, $k=3.06$ cm^{-1}, and hence this region corresponds to capillary waves. The capillary spectrum exhibits a power law dependence[14] and we assume the following form:

$$F(\boldsymbol{K},\boldsymbol{n}) = A_m (K_m/K)^q (1+A_r \cos 2\Psi) \times (1+BS_u/\bar{S}_u) u(K-K_c) \tag{4}$$

The leading term A_m is the zeroth-order azimuthal harmonic of the wavenumber spectrum at the point of minimum phase speed given by $K_m=3.63$ cm^{-1}. The exponent q is the power law, and A_r is the ratio of the first-order harmonic to the zeroth-order harmonic and is assumed independent of K. The quantity Ψ is the angle between $\boldsymbol{K}$ and the projection of the friction-velocity vector $\boldsymbol{U}_*$ onto the plane orthogonal to $\boldsymbol{n}$.

$$\cos\Psi = \boldsymbol{K}\cdot\boldsymbol{n}\times(\boldsymbol{U}_*\times\boldsymbol{n})/[K|\boldsymbol{n}\times(\boldsymbol{U}_*\times\boldsymbol{n})|] \tag{5}$$

The straining of small waves by the orbital motion of larger waves is accounted for in Eq. (4) by the third term in parentheses. This term weights the spectrum according to the upwind regional slope S_u. A positive straining coefficient B means that regions on the downwind slope of a large wave have a higher capillary spectrum than regions on the upwind slope. The last term in Eq. (4) is a unit step function that cuts the spectrum off to zero for all wavenumbers less than the cutoff wavenumber K_c. This term is necessary because sea waves longer than the dimensions of the scattering regions do not contribute to the regional wavenumber spectrum, although they are responsible for the tilting of the regions.

Wentz[11] found that the spectral amplitude A_m and the rms regional slope $\bar{S}=(\bar{S}_u^2+\bar{S}_c^2)^{1/2}$ are highly correlated with the friction velocity U_*. The correlations are expressed as

$$\log A_m = a_0 + a_1 \log U_* \tag{6}$$

$$\bar{S} = s_0 + s_1 \log U_* \tag{7}$$

where A_m is in cm^4 and U_* is in cm/s. The upwind and crosswind rms slopes, $\bar{S}_u$ and $\bar{S}_c$, are found from $\bar{S}$ by introducing an additional parameter $\rho=\bar{S}_c/\bar{S}_u$. This parameter and the other parameters appearing in Eq. (4) exhibit little or no correlation with U_*.

Table 1 gives the values for the ten model parameters appearing in the above formulation. These values are obtained by fitting the model, in a least-squares sense, to the vertical polarization NRCS aircraft measurements of known wind-sea states discussed in the previous section.

The rms difference between the model and the measurements is 0.7 dB. The regression coefficients, a_0 and a_1, for the amplitude of the capillary spectrum are in excellent agreement with the values -8.43 and 2.25 derived by Mitsuyasu and Honda [Ref. 14, Eqs. (13) and (25)] from capillary spectrum measurements in a wind-wave channel. Applying the regression Eq. (7) to Cox and Munk's[13] clean surface slope data yields values of 0.049 and 0.116 for s_0 and s_1. The difference between these values and the values deduced from the NRCS measurements is probably due, in part, to the fact that our slopes are only for sea waves having wavenumbers less than the cutoff wavenumber K_c. Cox and Munk also found the ratio of the crosswind to the upwind rms slope to be 0.87, which compares favorably to our value of 0.93. The capillary power law of 4.9 is in fair agreement with Phillips'[15] value of 4 for an idealized capillary spectrum. The capillary spectrum is highly anisotropic as is indicated by the large

Table 1 Dimensionless NRCS model parameters

Parameter	Value
a_0	-8.8
a_1	2.3
s_0	0.071
s_1	0.078
ρ	0.93
q	4.9
A_r	0.61
B	0.20
K_c/k	0.66
R	0.41

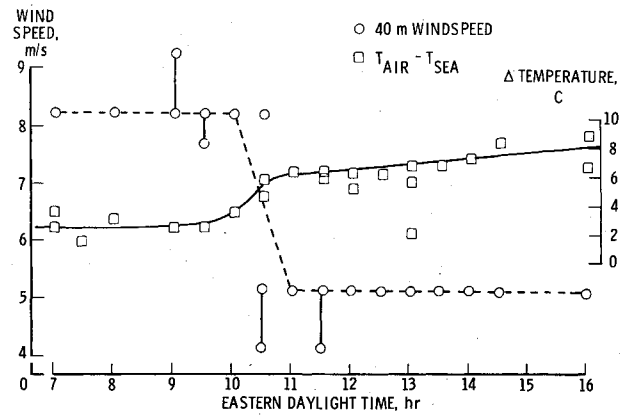

Fig. 4 Ground truth measurements at Ambrose Tower for the April 17, 1975 MESA experiment.

value for A_r. In addition, a positive straining coefficient B indicates that the capillary spectrum is the highest on the downwind slopes of the larger waves. This result is in agreement with Keller and Wright's wave tank experiment.[16] The cutoff wavenumber K_c is about two-thirds the radiation wavenumber. Finally, the power reflection coefficient R is 0.41 compared to a value of 0.61 for the Fresnel power reflectivity. It thus appears that the capillary waves reduce the reflected power by about one-third.

Once all the NRCS model parameters have been assigned values, the only remaining variables are the observation vector $\boldsymbol{k}_i$ and the friction velocity vector $\boldsymbol{U}_*$. In particular, the NRCS is a function of the friction velocity magnitude U_*, the incidence angle θ, and the relative azimuth angle ψ between $\boldsymbol{U}_*$ and the projection of $\boldsymbol{k}_i$ onto the mean surface.

$$\cos\theta = -\boldsymbol{k}_i\cdot\boldsymbol{N} \tag{8}$$

$$\cos\psi = \boldsymbol{N}\times(\boldsymbol{k}_i\times\boldsymbol{N})\cdot\boldsymbol{U}_*/[|\boldsymbol{N}\times(\boldsymbol{k}_i\times\boldsymbol{N})|\,U_*] \tag{9}$$

The NRCS in functional form is then denoted by $f(\theta,\psi,U_*)$.

Algorithm for Computing the Friction Velocity Vector

We now consider the situation in which several NRCS measurements are taken of the same wind-sea state and want to find the probability $P(\boldsymbol{U}_*|\{\sigma_n^0\})$ that the friction velocity has a value $\boldsymbol{U}_*$ given the set $\{\sigma_n^0\}$ of n measurements. This probability is given by the following extension of Bayes' equation:

$$P(\boldsymbol{U}_*|\{\sigma_n^0\}) = \frac{P(\boldsymbol{U}_*)\prod_{i=1}^{n} P(\sigma_i^0|\boldsymbol{U}_*,\{\sigma_{i-1}^0\})}{\int d\boldsymbol{U}_* P(\boldsymbol{U}_*)\prod_{i=1}^{n} P(\sigma_i^0|\boldsymbol{U}_*,\{\sigma_{i-1}^0\})} \tag{10}$$

The term $P(U_*)$ is the probability that the friction velocity vector is U_* independent of the NRCS measurements. We assume that no other information on U_* is available and let $P(U_*)$ be a uniform distribution over U_* space. Hence, $P(U_*)$ can be removed from the integral and cancels out.

The other term $P(\sigma_i^0 | U_*, \{\sigma_{i-1}^0\})$ in Eq. (10) is the probability that the ith measurement has a value of σ_i^0 given the friction velocity vector is U_* and the first through $i-1$ measurements are the set $\{\sigma_{i-1}^0\}$. In order to specify $P(\sigma_i^0 | U_*, \{\sigma_{i-1}^0\})$, an analysis of the fluctuations in the aircraft NRCS measurements was performed. These fluctuations are caused by the microscale turbulence in the wind field and by the scatterometer noise. A χ^2 test indicated that the distribution of the measurements is closer to log-normal than normal. In view of this we assume that σ_i^0 is log-normally distributed about the actual NRCS given by the function $f(\theta_i, \psi_i, U_*)$ discussed in the previous section. The angles θ_i and ψ_i are the incidence and relative azimuth angle for the ith measurement. Under this assumption $P(\sigma_i^0 | U_*, \{\sigma_{i-1}^0\})$ is independent of $\{\sigma_{i-1}^0\}$ and is given by

$$P(\sigma_i^0 | U_*, \{\sigma_{i-1}^0\}) = (2\pi\delta_i^2)^{-1/2} \exp\{-[\bar{\sigma}_i^0 - \bar{f}_i(U_*)]^2 / 2\delta_i^2\} \tag{11}$$

where $\bar{\sigma}_i^0 = \log \sigma_i^0$, $\bar{f}_i(U_*) = \log f(\theta_i, \psi_i, U_*)$, and δ_i is the standard deviation of $\bar{\sigma}_i^0$. Substituting Eq. (11) into Eq. (10) yields

$$P(U_* | \{\sigma_n^0\}) = \frac{\prod_{i=1}^{n} \exp\{-[\bar{\sigma}_i^0 - \bar{f}_i(U_*)]^2 / 2\delta_i^2\}}{\int dU_* \prod_{i=1}^{n} \exp\{-[\bar{\sigma}_i^0 - \bar{f}_i(U_*)]^2 / 2\delta_i^2\}} \tag{12}$$

For a single, noise-free NRCS measurement, the possible friction velocity vectors lie on a line in U_* space. For the case of two orthogonal, noise-free measurements, i.e., $\psi_2 = \psi_1 + 90$ deg, the probability $P(U_* | \sigma_1^0, \sigma_2^0)$ is nonzero only at the intersections of the two lines corresponding to the individual measurements. The number of intersections ranges from one to four depending on the value of ψ_1. The presence of noise spreads the region of possible U_* over areas in the neighborhood of the intersection points. When there are more than two measurements, the situation becomes more complicated with many such areas possible.

In order to obtain a best estimate of the friction velocity vector, we find the set of U_* corresponding to the local maxima of $P(U_* | \{\sigma_n^0\})$. Some of the maxima may be much lower than the others and are discarded. If additional meteorological data of sufficient quality are available on wind direction, then in principle all the remaining U_* can be eliminated except for the one corresponding to the actual friction velocity vector. The local maxima are found by first setting to zero the derivative of $P(U_* | \{\sigma_n^0\})$ with respect to U_* for a particular friction velocity direction. Performing this operation on Eq. (12) gives

$$\sum_{i=1}^{n} \{[\bar{\sigma}_i^0 - \bar{f}_i(U_*)] / \delta_i^2\} \bar{f}_i'(U_*) = 0 \tag{13}$$

where the prime denotes differentiation with respect to U_*. We next use the property that for incidence angles greater than 20 deg an approximate linear relationship exists between $\bar{f}_i(U_*)$ and $\log U_*$. Taylor's expansion gives

$$\bar{f}_i(U_*) = \bar{f}_i(U_*^0) + (\log U_* - \log U_*^0) \bar{f}_i'(U_*^0) + \Delta \tag{14}$$

where U_*^0 is a first guess for the friction velocity vector and Δ is the remainder term. The prime now denotes differentiation with respect to $\log U_*$. Setting the remainder term to zero and substituting Eq. (14) into Eq. (13) yields on the first iteration

$$\log U_*^1 = \log U_*^0 + \frac{\sum_{i=1}^{n} [\bar{\sigma}_i^0 - \bar{f}_i(U_*^0)] \bar{f}_i'(U_*^0) / \delta_i^2}{\sum_{i=1}^{n} [\bar{f}_i'(U_*^0)]^2 / \delta_i^2} \tag{15}$$

On the second iteration U_*^1 replaces U_*^0 in Eq. (15) and a U_*^2 is found. The procedure continues until the desired convergence is reached. Generally only one or two iterations are required for a convergence of 0.5 dB in $\log U_*$.

Equation (15) is used to find a U_{*j} for friction velocity directions from 0 to 359 deg in 1-deg steps, yielding a set of 360 friction velocity vectors. The corresponding probabilities $P(U_{*j} | \{\sigma_n^0\})$ are searched for local maxima. If the jth probability is greater than or equal to the $j-1$ and $j+1$ probabilities, then U_{*j} along with its probability are outputted. In this way we find the set of U_* corresponding to the local maxima of $P(U_* | \{\sigma_n^0\})$.

MESA Experiment

On April 17, 1975, an aircraft experiment was conducted in the New York Bight.[17] The objective of this experiment was to demonstrate the viability of the radar remote sensing technique for the measurement of the ocean-surface wind vectors and to provide these measurements at selected sites for the investigation of the wind-induced ocean currents in the bight. NRCS measurements were obtained using the AAFE RADSCAT 13.9-GHz scatterometer operating on a C-130 aircraft (NASA-929). RADSCAT was configured so that the antenna scanned to the left side normal to the aircraft ground track. During the measurements, the aircraft performed a series of counterclockwise 360-deg turns (20-deg bank angle), while the antenna was pointed at an elevation angle of 50 deg from the aircraft vertical axis. This maneuver permitted the antenna to illuminate approximately the same surface area (center of circle) while undergoing continuous azimuth rotation. The polarization was transmitted horizontal and received horizontal, and the incidence angle was 30 deg.

In this experiment, radar data taken during four circular flight patterns at preselected sites were processed to produce the average NRCS measurements as a function of azimuth angle. Also, wind speed, wind direction, air temperature, and sea temperature were recorded every half hour at the United States Coast Guard Ambrose Tower located in the New York Bight. These measurements were used to provide surface truth for verifying the RADSCAT inferred wind vectors. The flight was conducted so that the first and last series of circles would occur at Ambrose Tower to provide a direct comparison of RADSCAT measurements with in situ data.

The wind speed measured at 40 m and the air-sea temperature difference recorded at the Ambrose Tower are plotted versus time in Fig. 4. The wind speed shows a sharp drop at 10:30 EDT and then remains constant while the air-sea temperature difference steadily increases. The friction velocity U_* and the 19.5-m neutral stability wind speeds are computed from the Ambrose Tower data using Cardone's atmospheric stability model.[10]

Friction velocities and directions are also derived from the aircraft NRCS measurements using the algorithm discussed in the previous section. As mentioned above, all the MESA measurements are horizontal polarization at an incidence angle of 30 deg. The model parameters for the NRCS function used by the algorithm are derived from vertical polarization measurements obtained during the JONSWAP experiment.¶ When they are used to compute the NRCS for horizontal polarization a bias with the JONSWAP measurements oc-

¶This procedure has since been modified such that both the vertical and horizontal NRCS measurements are used separately to estimate the model parameters for the SeaSat-A wind algorithm.

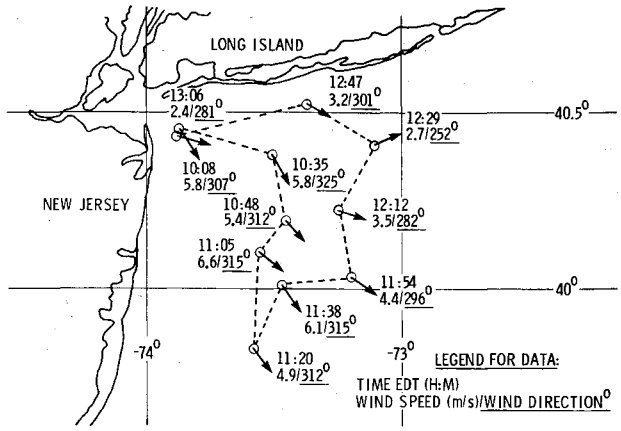

Fig. 5 RADSCAT measurement sites for the April 17, 1975 MESA experiment showing wind vector data deduced using data base of Ref. 5.

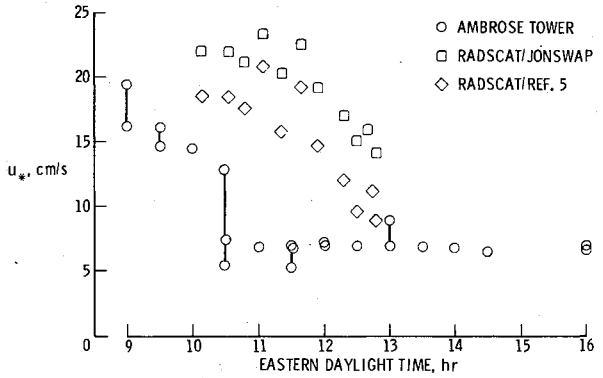

Fig. 6 Comparison of frictional velocity U_* inferred from NRCS with ground truth for the April 17, 1975 MESA experiment.

curred. The measurements are higher than the computations for incidence angles of 30 deg and greater. One possible explanation for this bias is that the crest of sea waves significantly contribute to the horizontal polarization backscattering. To account for this effect, we increase the regression coefficient a_0 for the capillary spectrum. At an incidence angle of 30 deg, the coefficient is increased by 1.6 dB in order to match the JONSWAP measurements.

The NRCS measurements obtained during the Gulf of Mexico flights[5] are about 3.6 dB higher than the JONSWAP measurements for horizontal polarization, an incidence angle of 30 deg, and light winds. The reason for this is not understood; therefore, we consider a second case in which the data base for the U_* algorithm is the Gulf of Mexico NRCS measurements rather than the JONSWAP NRCS measurements.

The results of the U_* algorithm are shown in Figs. 5, 6, and 7. In Fig. 5 the friction velocities are converted to 19.5-m neutral stability wind speeds and are the values obtained using the Gulf of Mexico NRCS data base. The computed wind speeds decrease as the flight progresses, and the wind direction shows a slight shift. Figure 6 compares the friction velocity obtained from the U_* algorithm with that obtained from the Ambrose Tower data. The squares are the friction velocities outputted by the algorithm when the JONSWAP data base is used and the diamonds are the values resulting from the Gulf of Mexico data base. The U_* that the algorithm computes from the NRCS measurements decreases with time, as does the Ambrose Tower U_*. The agreement in magnitude is very good at the end of the flight when the aircraft was in the vicinity of the tower. At other times when the aircraft and tower measurements are not spatially simultaneous (Fig. 5) the disagreement is poorer, as is to be expected. Also using the two different data bases for the U_* algorithm results in about

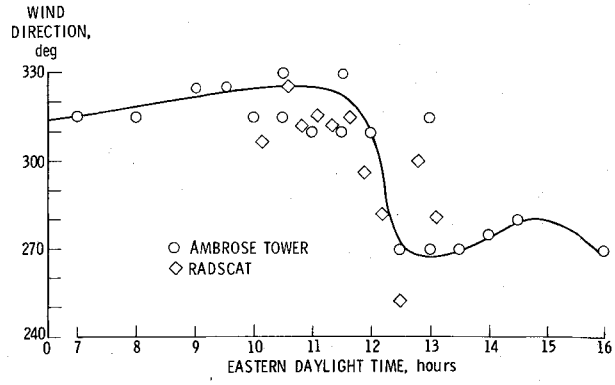

Fig. 7 Comparison of wind direction inferred from NRCS with ground truth for the April 17, 1975 MESA experiment.

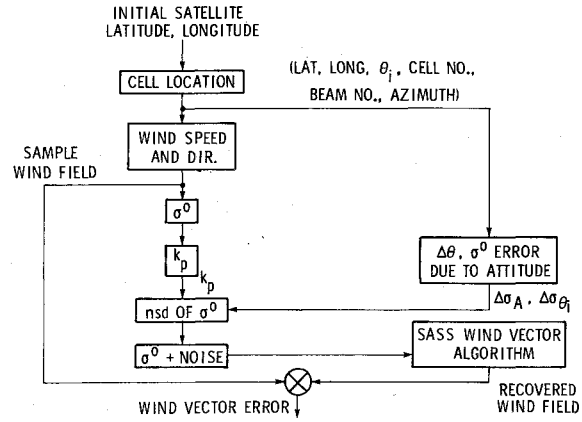

Fig. 8 Flow diagram of SASS NRCS conversion to wind vector.

a 4-cm/s difference in the computed friction velocity. Further, for this experiment, the air-sea temperature difference indicated extremely stable air in light, unsteady winds. This is a difficult case for surface boundary-layer models to accurately compute, and therefore the calculated U_* could easily be biased by 10-20% for these conditions. Figure 7 compares the wind direction obtained from the Ambrose Tower. The algorithm gives essentially the same wind direction results for the two data bases. A curve is faired through the tower wind directions and compares favorably with the algorithm directions.

Wind Field-Simulated SASS σ^0 Inversion

In order to test the ability of the SASS wind vector algorithm to convert satellite NRCS measurements to winds, a simulation of the data reduction process was carried out. The simulation followed the flow diagram given in Fig. 8. In summary, a test wind field was selected and NRCS "measurements" were calculated from the NRCS function $f(\theta,\psi,U_*)$. These NRCS values were then contaminated with communication noise and other random errors and the results inverted using the SASS wind vector algorithm.

The test wind field selected was an extratropical cyclone over the North Atlantic. This wind field is shown in Fig. 9. Wind speed and direction were specified every degree of latitude and longitude on a 20×20-deg grid, and every ½ deg on a 12×12-deg grid within the larger grid. The higher density grid was used where the wind field exhibited large gradients. Using a computer program which simulates the SASS operation in orbit, the satellite was "passed" over the wind field in a mode such that measurements were made on both sides of the spacecraft in vertical polarization only. As a part of the program, the range and location (and other parameters) of the center of the Earth-located SASS resolution cells were calculated. Only data from the right side were used for this case and their location on the wind field are shown in Fig. 9. The wind speed and direction from the grid points of the test

Table 2 Summary of SASS simulation results

Algorithm		Wind speed results: Number of solutions	Wind speed results: Rms error	Wind speed results: % within user limits	Wind direction results: Number of solutions	Wind direction results: Rms error, deg	Wind direction results: % within user limits
Noise-free	<20 m/s	479	0.97 m/s	92.3	...	...	...
	>20 m/s	33	7.85%	81.8	...	...	...
	Combined	512	1.03 m/s	91.6	512	8.58	95.5
Noise-added	<20 m/s	452	1.32 m/s	88.9	...	...	...
	>20 m/s	32	9.77%	75.0	...	...	...
	Combined	484	1.39 m/s	88.0	484	16.90	84.7

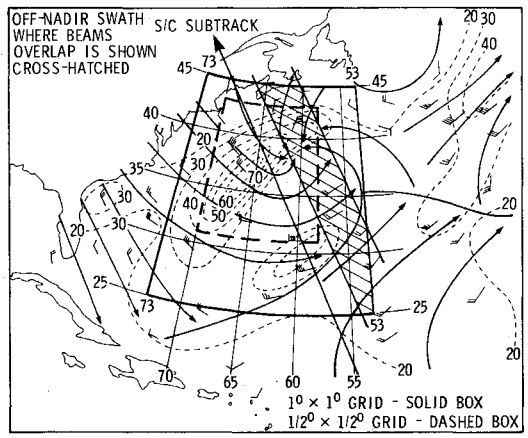

Fig. 9 Wind field used in SASS simulation experiment.

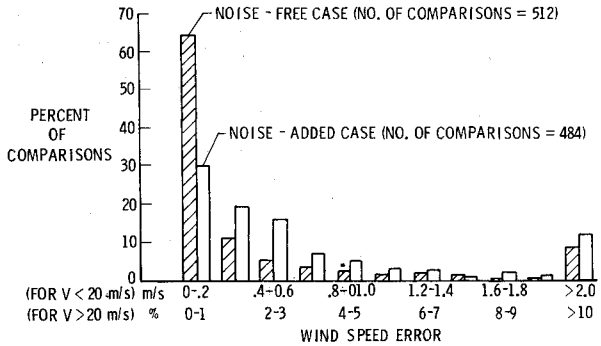

Fig. 10 SASS simulation statistics of wind speed error.

wind field were then interpolated to the center of each SASS resolution cell. Next, the NRCS was calculated from $f(\theta,\psi,U_*)$. Subsequently, the estimated normalized standard deviation due to communication noise (Kp) was calculated for each simulated SASS σ^0 measurement, and the Kp error was combined with random errors from other sources[4] to arrive at a simulated "total measurement error" for the nominal orbit conditions. This error was added randomly to the "noise-free" NRCS to simulate data that would be received by SASS. Both the noise-free and the noise-added NRCS "measurements" were supplied to the SASS wind vector algorithm for inversion to wind speed and direction.

The SASS wind vector algorithm sets up an Earth-fixed grid and for each grid point groups all measurements which lie within 50 km. For this case, the Earth-fixed grid was at ½-deg grid points for the whole wind field. The group of measurements serves as inputs for the U_* algorithm. The algorithm then outputs a list of probable U_*, which are converted to neutral stability winds. The algorithm generally predicts four or less solutions for each grid point which are nearly equal in wind speeds, but which vary widely in direction. This result has been referred to as aliasing and must be removed by further processing (not considered here). For the present case, a prior knowledge of wind direction is

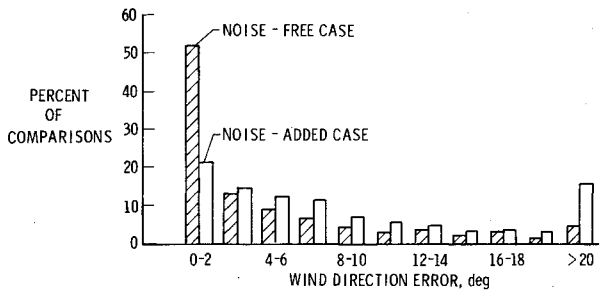

Fig. 11 SASS simulation statistics of wind direction error.

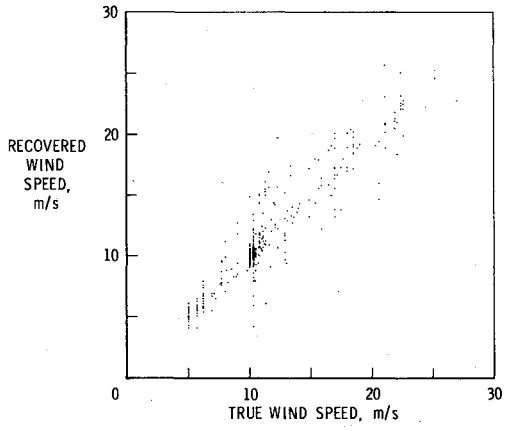

Fig. 12 SASS simulation wind speed, recovered vs true, noise-added case.

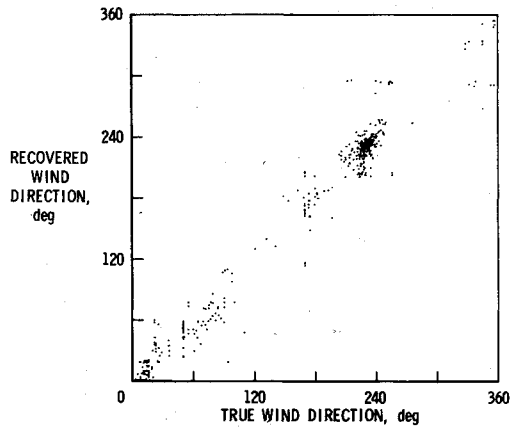

Fig. 13 SASS simulation wind direction, recovered vs true, noise-added case.

assumed, and therefore the comparisons are made with the solution having the closest direction to the true direction.

Recovered and true wind speed and direction were compared for both the "noise-free" and "noise-added" cases. These results were then compared to user requirements (wind speed = ±2 m/s or 10%, whichever is larger; wind direction = ±20 deg).

Figures 10 and 11 show these comparisons in histogram form. The abscissa is divided into 11 bins, the first 10 of which are 1/10 of the user requirements in size and the eleventh contains all results outside. For the wind speed results (Fig. 10), the noise-free results appear quite good, with 65% of the results within the first bin and all but 8.4% within user requirements. For the noise-added case, the vast majority of the results are contained in the first 5 bins (± 1 m/s or $\pm 5\%$), and all but 12% of the results are contained within user requirements. Wind direction results (Fig. 11) show the same general trends. Noise-free results show that 95.5% of the cases are within user requirements, with 52% within 2 deg. Noise-added results are spread more widely, but still 85% of the cases are within user limits. It is emphasized that this comparison uses the recovered wind vector solution known to be closest in direction. Hence, an "alias removing" technique is required before these statistics are meaningful. Table 2 gives a summary of the results, including the rms error.

These results are presented in another form in Figs. 12 and 13. Here, the recovered wind speeds and wind directions are plotted against the true conditions, with desired results being a 45-deg line-of-perfect-agreement. It can be seen that the results group around the 45-deg line quite well.

Concluding Remarks

The sea-surface NRCS model, which is based on two-scale scattering theory, is in good agreement with measured data collected in the North Sea, the Atlantic Ocean, and the Gulf of Mexico. The average rms difference between the model and the North Sea measurements is 0.7 dB. Confidence in the model is further bolstered by the fact that the model's geophysical parameters correspond quite closely to parameters independently measured by oceanographic experiments. The inversion algorithm for computing the friction-velocity vector from a group of NRCS measurements is based on an extension of Bayes' equation and is, in effect, a maximum likelihood estimation.

The MESA experiment is used to test the algorithm. This is a particularly difficult test in that the winds were light and fluctuating. Even so, the algorithm performed well, giving friction-velocity vectors in good agreement with the measured ground truth. In this test two different NRCS functions are used by the algorithm. The first function is based on North Sea NRCS measurements, and the second on Gulf of Mexico measurements. The computed friction velocities differ by about 4 cm/s depending on which function is used. This fact suggests the need for collecting NRCS measurements in conjunction with ground truth on a global basis.

As a further test of the algorithm, a SASS simulation study is performed. The simulated NRCS measurements are obtained by passing the satellite over an extratropical cyclone in the North Atlantic. The NRCS values, contaminated with communication noise and other random errors, are then inverted by the algorithm. These results indicate that the users' requirements on wind speed are satisfied 88% of the time. For the case of wind directions the users' requirements are met 85% of the time, provided that the aliases can be removed.

References

[1] "The Terrestrial Environment: Solid Earth and Ocean Physics," *Williamstown Report*, M.I.T., Cambridge, Mass., NASA CR-1579, April 1970.

[2] McCandless, S. W. and Cardone, V. J., "SeaSat-A Oceanographic Data System and Users," *I.A.F. 27th Congress*, Anaheim, Calif., Oct. 10-16, 1976.

[3] Apel, J. R., "A Hard Look at Oceans from Space," *AIAA 9th Annual Meeting and Technical Display*, Washington, D. C., Jan. 8-10, 1973.

[4] Grantham, W. L., Bracalente, E.M., Jones, W.L., and Johnson, J.W., "The SeaSat-A Satellite Scatterometer," *IEEE Journal of Oceanic Engineering*, Vol. OE-2, April 1977, pp. 200-206.

[5] Jones, W. L., Schroeder, L. C., and Mitchell, J. L., "Aircraft Measurements of the Microwave Scattering Signature of the Ocean," *IEEE Journal of Oceanic Engineering*, Vol. OE-2, April 1977, pp. 52-61.

[6] Daley, J., "Wind Dependence of Radar Sea'Return," *Journal of Geophysical Research*, Vol. 78, Nov. 1973, pp. 7823-7833.

[7] Krishen, K., "Correlation of Radar Backscattering Cross Sections with Ocean Wave Height and Wind Velocity," *Journal of Geophysical Research*, Vol. 76, Sept. 1971, pp. 6528-6539.

[8] Cardone, V. J. et al., "The Measurement of the Winds Near the Ocean Surface with a Radiometer – Scatterometer on Skylab," NASA Johnson Space Center, Houston, Tex., final report on EPN 550 Contract No. NAS-9-13642, Jan. 1976.

[9] Jones, W. L. and Schroeder, L. C., "Radar Backscatter from the Ocean: Dependence on Surface Friction Velocity," *Boundary Layer Meteorology*, Vol. 13, 1978, pp. 133-149.

[10] Cardone, V. J., "Specification of the Wind Distribution in the Marine Boundary Layer for Wave Forecasting," New York University School of Engineering and Science, University Heights, N. Y., TR 69-1, March 1970 (available as DDS AD 702490).

[11] Wentz, F. J., "Two Scale Scattering Model with Application to the JONSWAP '75 Aircraft Microwave Scatterometer Experiment," NASA CR-2919. 1977.

[12] Wentz, F. J., "Radar Backscattering from a Sea Having an Anisotropic Large-Scale Surface," NASA CR-145278, 1977.

[13] Cox, C. and Munk, W., "Slopes of the Sea Surface Deduced from Photographs of Sun Glitter," *Bulletin of Scripps Institute of Oceanography*, Vol. 6, No. 9, 1956, pp. 401-488.

[14] Mitsuyasu, H. and Honda, T., "The High Frequency Spectrum of Wind Generated Waves," *Journal of the Oceanographical Society of Japan*, Vol. 30, Aug. 1974, pp. 185-198.

[15] Phillips, O. M., *The Dynamics of the Upper Ocean*, Cambridge University Press, London, 1966.

[16] Keller, W. C., and Wright, J. C., "Modulation of Microwave Scattering and the Straining of Wind-Generated Waves," *Radio Science*, Vol. 10, Feb. 1975, pp. 139-147.

[17] Hall, J. B. Jr. and Pearson, A. O., "Results from the National Aeronautics and Space Administration Remote Sensing Experiments in the New York Bight – April 7-17, 1975," NASA TMX-74032, 1977.